

Stratospheric Gravity Wave Simulation over Greenland during 24 January 2005

Varavut Limpasuvan

Department of Chemistry and Physics, Coastal Carolina University, Conway, South Carolina

Dong L. Wu

NASA Jet Propulsion Laboratory, California Institute of Technology, Pasadena, California

M. Joan Alexander

Colorado Research Associate Division, NorthWest Research Associates, Inc., Boulder, Colorado

Ming Hu and Ming Xue

Center for Atmospheric Prediction Systems, University of Oklahoma, Norman, Oklahoma

Steven Pawson

Global Modeling and Assimilation Office, NASA Goddard Space Flight Center, Greenbelt, Maryland

James R. Perkins

Department of Computer Sciences, Coastal Carolina University, Conway, South Carolina

Abstract. The *Advanced Regional Prediction Systems* (ARPS) forecast model is extended up to the stratopause and over the entire hemisphere to simulate gravity waves during 24 January 2005. With a 15-km (0.4-km) horizontal (vertical) resolution, the simulation produces realistic gravity wave features related to geostrophic adjustment of tropospheric jet and topographical flow over the Greenland terrain, when a near-surface high pressure system is present over the North Atlantic. In the stratosphere, wave signatures appear near the region of strongest flow in the polar vortex, where negative vertical flux of horizontal momentum is pronounced. Flux divergence associated with horizontal flow acceleration of $12\text{-}120\text{ m s}^{-1}\text{ day}^{-1}$ coincides with areas of depleted stratospheric wind speed, suggesting strong interactions between gravity waves and the polar vortex. Simulated temperature wave perturbations compare favorably with radiance perturbation from NASA AIRS observations. Coarser simulation using 50-km horizontal resolution produces gravity waves of significantly weaker amplitudes.

1. Introduction

Gravity waves are generated mainly by tropospheric processes such as convection, jet stream instability [Nappo, 2002], and flow over topography [Eckermann and Preusse, 1999]. While we recognize their importance in maintaining the atmospheric structure above the troposphere [Fritts and Alexander, 2003; and references therein], our understanding of their properties is still limited. With oscillatory periods as short as several minutes and spatial scales on the order of 10-1000 km, gravity waves are difficult to observe either globally with satellite measurements [e.g. McLandress *et al.*, 2000; Wu, 2004] or locally with sounding measurements. This difficulty is exacerbated by gravity wave's intermittent nature due to variations in generating sources and flow conditions.

With computational grid sizes that are still too coarse to explicitly resolve very small scale features, present climate models must include gravity wave effects through parameterization schemes that specify gravity wave sources and estimate wave dissipation at higher altitudes [e.g. Lindzen, 1981]. However, because of observational uncertainties, wave sources and wave dissipation are still poorly understood and not well quantified. To simulate proper climatology of the atmosphere, climate modelers must haphazardly fine tune these schemes [Fritts and Alexander, 2003]. Consequently, differing conclusions can be drawn from these modeling results. Because climate models are indispensable tools in assessing present and future climate variations, greater details about gravity wave properties are needed to better constrain how they are specified in these models.

Here, we demonstrate the usage of a compressible, non-hydrostatic weather forecast model called the *Advanced Regional Prediction Systems* (ARPS, version 5.0.0) [Xue *et al.*, 2000; Xue *et al.*, 2003] as a possible tool for simulating realistic gravity waves up to

the stratopause. Modeling results can potentially provide greater details about gravity wave properties and help improve physical constraints on how these waves are treated in future climate models. In particular, we highlight gravity wave features centered near Greenland during 24 January 2005. We track the wave appearance to their possible source in the troposphere and diagnose the wave influence on the polar vortex strength. *Horinouchi et al.* [2002] successfully employed this model to study convectively generated gravity waves propagating into the middle atmosphere. However, that ARPS-based study was conducted under an idealized scenario using a much smaller horizontal domain with periodic horizontal boundaries and a single sounding to describe the initial vertical variations. No realistic terrain was used either. In this study, we showcase a simulation with realistic conditions in the troposphere and stratosphere, focusing on gravity waves related to topography and jet variations.

2. Model Set-up

Unless specified otherwise, the ARPS model horizontal resolution and time step are set to 15 km and 10 seconds, respectively. The model uses a generalized terrain-following coordinate in which the computational grid is defined by transformation Jacobians that are numerically determined by the model. In our set-up, the vertical grid spacing is specified to be 20 m in the lowest level and gradually increases with altitude to 400 m at 12 km, above which the vertical grid spacing remains fixed and the coordinate surfaces flattened. The bottom boundary condition is rigid and represents realistic terrain over the domain of the simulation. The global terrain height source is the 30 arc second USGS data set (approximately 0.920 km in latitude and $0.920 \times \cos(\text{latitude})$ km in longitude). Surface physics is turned on with surface fluxes (over land and water) calculated from stability-dependent surface drag coefficient and predicted surface

temperature and water content [Businger *et al.*, 1971; Byun, 1990]. Surface characteristics (soil types and vegetation data) are obtained from the Global Ecosystems Database (GED) Version 1.0 from NOAA's National Geophysical Data Center (NGDC). A simple 2-layer soil model is based on *Noilhan and Planton* [1989] scheme. The Goddard Earth Observation System, Version 4 [GEOS-4; *Bloom et al.*, 2005] global reanalysis data from NASA's Global Modeling and Assimilation Office [GMAO; *Rienecker*, 2004] is used for model initialization. Every six hours, the GEOS-4 data are given on a $1.25^\circ \times 1.0^\circ$ global longitude-latitude horizontal grid and extends upward to about 0.01 hPa.

The microphysics scheme (with ice phase) of *Lin et al.* [1983] represents the model's moist processes. Cumulus convection is parameterized by the scheme of *Kain and Fritsch* [1993]. The combined usage of microphysics and cumulus convection parameterizations has been used successfully in similar medium-scale modeling of gravity waves [e.g. *Muturilli and Dörnbrack*, 2006]. The 1.5-order turbulent-kinetic-energy-based scheme [e.g. *Deardorff*, 1980] provides the subgrid-scale closure for turbulence mixing (eddy diffusion). A full radiative calculation is implemented every 100 seconds. The treatment of shortwave and long-wave radiation is based on *Chou* [1990] and *Chou and Suarez* [1994], respectively. The Coriolis parameter is turned on in all simulations.

Initially, the simulation is run in a hemispheric mode (HM), centered over the Northern Hemisphere polar cap, with a rigid top boundary condition set at 38 km. This initial run surveys possible gravity wave activity over the entire hemisphere up to the lower stratosphere. To examine gravity waves up to the stratopause while keeping the simulation within our available computing resources, the second simulation is run in a regional mode (RM) of $8900 \text{ km} \times 7200 \text{ km}$ horizontal domain, with a rigid lid at 56 km.

This latter run focuses on areas where identifiable wave activities appear in the HM mode. For this regional setup, the model's lateral boundary condition is externally determined by the time-dependent GEOS-4 data. Relaxation (at rate of 0.002 s^{-1}) towards the external solution is imposed in a 200-km wide zone near the lateral boundaries to reduce potential large inconsistencies between the model solution and the external GEOS-4 data. In all simulations, the upper-level Rayleigh damping increases gradually with altitude from 0 at 32 km for HM and 50 km for RM to 0.033 s^{-1} at the model top. This damping strictly serves to prevent spurious wave reflection to the rigid top boundary. Results are saved every 6 minutes of simulation time.

3. Results

A. Planar View

The left panel of Fig. 1 shows a sample result of the HM simulation at 15 km horizontal resolution, valid at 1200 UTC, 24 January 2005 (i.e. 12 hours after initialization). At 10 hPa (near the upper boundary of the simulation that is unaffected by the Rayleigh damping), a well-defined polar vortex low is displaced slightly off the pole, with adjacent high geopotential height centers over the northern ocean regions. Strong vertical winds, with alternating bands of upward and downward motion, are present in association with gravity waves over the North Atlantic. For the simulation with a lower 50-km horizontal resolution (right panel of Fig. 1), a similar height field is shown. However, throughout the hemisphere, gravity waves are nearly absent in terms of the vertical velocity, when presented at the same contour interval.

To examine the North Atlantic gravity wave features at higher altitude, a RM simulation with 15-km horizontal resolution is performed for the domain centered over the southern tip of Greenland. Fig. 2 demonstrates that the ARPS simulation compares

very well with the GEOS-4 output at the same time (Fig. 2b and c). A ridge is situated over the North Atlantic (just off the coastline of Northern Europe) adjacent to an elongated trough over eastern Canada. Relative to the initial condition (0000 UTC), the ARPS simulated jet flow (Fig. 2c) over Greenland has migrated northward with a more pronounced curvature on the western side over Greenland at 1800 UTC than in the GEOS-4 output (Fig. 2b). The modeled flow, with much higher resolution, has also strengthened more during this period with horizontal wind speed exceeding 80 m s^{-1} over Greenland and the Labrador Sea. Simulated vertical winds at 80 hPa (superimposed on the simulation results as blue/red contours on Fig. 2c) are consistent with the perturbations shown in Fig. 1 over the North Atlantic.

Figure 3 shows the simulated tropospheric conditions (200 and 500 hPa levels) at 6 and 18 hours after initialization. South of Greenland, a cold front appears off the eastern U.S. coast, with strong temperature gradient (green contours) and intense bands of mid-tropospheric upward motion (red-filled contours). As time progresses, the frontal structure weakens and the jet exhibits more anti-cyclonic curvature (i.e. increasingly Ω -like in shape) near Greenland (see also Fig. 2).

Figure 4 demonstrates the same fields as Fig. 3 but in the stratosphere at the 2.5 and 50 hPa levels. The strong ridge observed over the North Atlantic in Fig. 3 is still evident at 50 hPa due to the elevated tropopause and anticyclone. As a result, the lower-stratospheric flow ($\sim 22 \text{ km}$) tends to be oriented in the same direction as the tropospheric jet around Greenland, favoring upward wave propagation. In the upper stratosphere (2.5 hPa), the flow is predominantly circumpolar, but the vortex is slightly displaced toward Greenland (see also Fig. 1).

Clusters of enhanced vertical wind perturbations (filled color contours) are present near or downstream of the Appalachians Mountains, Greenland, and the Pyrenees. In particular, wind perturbations associated with the Appalachians appear in two separate patches of wave activity: one over the Virginia Appalachians, and another north of Maine. However, the predominant vertical wind perturbations throughout the troposphere *and* stratosphere are those over much of eastern Greenland (where the flow tends to align at different levels). Clearly gravity waves, these perturbations have complex structures with wave fronts that are neither perfectly parallel nor perpendicular to the jet axis.

While relatively weak (with magnitude less than 2 m s^{-1}) at 80 hPa, vertical wind fluctuations are much stronger at higher altitude as result of amplitude amplification due to reduced atmospheric density. Within the polar vortex, the 2.5-hPa height contours are greatly distorted, suggesting horizontal overturning motion related to these waves.

B. Cross-sections

To elucidate gravity wave characteristics over the eastern part of Greenland, vertical cross-sections at AB slice (nearly perpendicular to the tropospheric jet) and CD slice (nearly parallel to the tropospheric jet) are examined. These slices are indicated in Figs. 3 and 4 as thick black lines near Greenland.

In Fig. 5 (AB slice), the jet (into the page of the cross-sections) below 20 km intensifies in time (exceeding 80 m s^{-1} by 1800 UTC) and shifts northwestward toward point A. The enhanced vertical wind perturbations (featured in the rectangular boxes of Fig. 5) are generally located above the jet core and shift slightly with the jet migration. The vertical and horizontal wavelengths of these wind perturbations are approximately 5-10 km and 200-300 km, respectively. The vertical scales increase slightly with altitude. Overall, these characteristics suggest that the perturbations shown in Fig. 4 are associated

with inertial-gravity waves [e.g. *Alexander and Fritts*, 2003]. Strong anti-cyclonic jet with pronounced curvature (Ω -shaped flow in our simulation; Figs. 3 and 4) can radiate inertial-gravity waves to maintain geostrophic balance [*Plougonven et al.*, 2003; *Plougonven and Snyder*, 2005]. The associated wave fronts tend to be parallel with the jet.

Wave perturbations over Greenland also appear to be related to orographic gravity waves. Around 1000 km from point C, wave perturbations as shown in Fig. 6 (CD slice) are of smaller horizontal wavelength (~80-150 km) than those shown in Fig. 5 and have vertical wavelength of 7-15 km. The wave structure is similar to those predicted by previous numerical studies of gravity wave generated by an isolated mountain ridge [e.g. *Xue and Thorpe*, 1991; *Xue et al.*, 2000]. Remaining relatively stationary in time, the zero vertical wind lines (wave nodes) in Fig. 6 tilt left with altitude, consistent with upward and upwind energy propagation. The overlaid isentropes (green contours) are highly perturbed. Local extrema of potential temperature values are in quadrature with the vertical winds. The vertical wave patterns appear to remain stationary relative to the terrain, and are strongest directly over the upwind slope (about 250 km from point C) and lee slope (about 1000 km from C), despite the northward shift (along the cross-sections) of the maximum wind (toward point D).

In particular, prevalent wave perturbations around 1000 km from point C are generated on the down slope of the Greenland terrain. Cold air over Greenland blowing down the terrain slope (“katabatic winds”) may potentially be the source of these orographic gravity waves. *Watanabe et al.* [2006] demonstrates that katabatic winds blowing off the Antarctic ice shelf can readily generate orographic gravity waves throughout Southern Hemisphere spring and winter. Fig. 6 suggests that katabatic winds

interacting with the eastern Greenland topography is a potential mechanism for the gravity waves in the ARPS simulation. However, steep lee slopes of mountain ranges are also locations known for large amplitude mountain waves that sometimes can create strong down slope winds [Lilly *et al.*, 1972; Xue *et al.*, 2000]. The jump in isentropes (the thick line) in Fig. 6 appears to have rather large amplitude.

As the jet-induced wave perturbations sit over the jet maximum, the model results suggest the overlaying of both inertial and orographic gravity waves near Greenland early in the simulation and the gradual separation of these two wave types with time. At 0600 UTC, the 200-hPa wave perturbations over Greenland seem to be a mixture of orographic waves and jet-triggered waves; horizontal wave fronts tend to be both perpendicular and parallel to the jet (Fig. 3). However, at 1800 UTC, most of the wave fronts appear to be more perpendicular to the flow and topographically generated. To this end, the simulated gravity waves are triggered at the earlier times by the intensifying jet (and geostrophic adjustment), and at the later times when jet is weaker, more gravity waves are topographically forced. Mountain waves require relatively strong low level flow, and are strongest on the slopes.

The possible combined existence of inertial-gravity waves and orographic gravity waves over Greenland in present simulation concur with the findings of *Maturilli and Dörnbrack* [2006] who note these wave features over Spitsbergen (Greenland) during 26 January 2005. Using MM5 model (with similar set-up as our model) extending up to about 25 km, they find over Spitsbergen the appearance of inertial gravity waves radiating away from the jet core (like Fig. 5c) that is followed by the presence of orographic gravity waves. During this transition, the local wave fronts that were initially parallel to the jet become perpendicular to the flow.

C. Wave Forcing

As time progresses from 0600 to 1800 UTC, the upper-level gravity wave amplitudes over Greenland have subsided considerably in section CD (Fig. 6). The amplitude decline can be associated with wave dissipation and the overlaying and subsequent separation of differing gravity wave types (discussed above). The diminishing wave amplitudes with time suggest possible wave influence on the background flow.

Figure 7 illustrates the changes in the horizontal wind speeds at 2.5 hPa with respect to the initial condition. In comparing the 1800 UTC GEOS-4 data with that of the simulation, it appears that, while the overall large scale flow has weakened in time, perturbations associated with gravity waves tend to cause additional localized deceleration of the overall flow. The wave influence is particularly evident between the shaded area and the reference CD slice, where chunks of the shaded regions have been carved away by the collocating wave activity. In this region, enhanced gravity wave activities are revealed by both strong vertical wind variations and the deformation of the 2.5-hPa geopotential height contours.

The possible influence of the simulated gravity waves on the upper stratospheric vortex is explored in Fig. 8. Here, the entire model domain is divided into 150-km \times 150-km sub-areas (i.e. 10-grid points \times 10-grid points squares). Vertical fluxes of momenta in the model's x direction (i.e. $\rho_o \overline{u'w'}$) and the y direction (i.e. $\rho_o \overline{v'w'}$) are computed for each of these areas. The overbar quantity represents an average over each sub-area, and the prime indicates the departure from that average. The variables u and v are the horizontal wind components in the model's x and y coordinates; w is the vertical wind. The computed flux for each sub-area is used to represent the value at the center of each sub-area box. The resulting central values (smoothed by a 2-point running mean) are

illustrated as contours in Fig. 8. Shown in the bottom row, the 1200 UTC fluxes at 2.5 hPa are nearly all negative with maximum amplitudes of $50 \times 10^{-3} \text{ kg m}^{-1} \text{ s}^{-2}$ in the x -momentum flux and coincide very well with the wave patterns shown in previous figures.

The vertical convergence of these fluxes (divided by ρ_o) is computed to diagnose the local wave forcing on the horizontal wind in the x and y directions (F_x and F_y , respectively):

$$(F_x, F_y) = -\frac{1}{\rho_o} \frac{\partial}{\partial z} (\rho_o \overline{u'w'}, \rho_o \overline{v'w'}).$$

As shown in the top row of Fig. 8, the predominant wave forcing tends to occur to the right of the reference CD slice. At 1200 UTC, the magnitude of the deceleration in the x -direction (y -direction) can reach nearly 0.5 (5) $\text{m s}^{-1} \text{ hour}^{-1}$. The location of the wave decelerative effects corresponds very well with the depleted wind speed shown in Fig. 7 at a slightly later time. This lag correlation (due to the influence of wave driving on wind tendencies) suggests that gravity wave dissipation in the model can interact with the polar vortex by locally slowing down the horizontal flow.

We note that the dissipation mechanism may not be realistic (i.e. too large) in the model. However, the decelerative effects are consistent with the wave forcing related to orographic gravity waves. In their examination of katabatic wind generation of orographic gravity waves over Antarctica polar vortex during winter, *Watanabe et al.* [2006] determines the localized deceleration of westerly winds to be greater than $30 \text{ m}^{-1} \text{ s}^{-1} \text{ day}^{-1}$ in the middle atmosphere due to wave dissipation. This forcing, in turn, exerts notable influence on the horizontal circulation of the polar vortex. In the present study, we estimate the deceleration to be about $12\text{-}120 \text{ m}^{-1} \text{ s}^{-1} \text{ day}^{-1}$. However, we caution that the size of the sub-area used in the above calculation does affect the detailed structure and

amplitudes of the results shown here. In particular, when the sub-area size is increased, the amplitudes shown in Fig. 8 weaken and structure of the contours becomes less detailed, as expected. Regardless, the presented results remain qualitatively unchanged. Finally, while the forcings may appear large, this deceleration effect may not be persistent for the entire day and the effect is not exerted on the same air parcels – the air stream passes through this region of quasi-stationary orographic waves.

D. Satellite Comparisons

We observe concurrent gravity waves over the North Atlantic using radiance perturbations from AIRS aboard NASA AQUA satellite [Aumann *et al.*, 2003; Fetzer *et al.*, 2003]. AIRS radiances in the CO₂ 15-micron band can be used to detect perturbations induced by gravity waves using the 2-D mapping technique discussed by Wu and Zhang [2004]. Initially, we find the AIRS “background state” by fitting cross-(satellite)-track radiance with a third-order polynomial function. We then smooth the fitted result along the satellite tracks with a 500-km running window. The radiance perturbations (assumed to be waves) are defined as the difference between this AIR background and the observed radiance. While AIRS has a horizontal resolution of ~15 km, it can only detect gravity waves with vertical wavelengths > 12 km [Alexander and Barnett, 2006]. Figure 9c shows the gravity waves observed by AIRS during 24 January 2005 at 2.5 hPa. Note that a spectral high-pass filter (keeping features smaller than 500 km) has been applied to the AIRS observations.

To compare with AIRS observations, the modeled temperature perturbations must be convolved (“blended”) with the broad vertical AIRS weighting functions corresponding to the 15-micron band. The convolution process reduces wave amplitudes substantially. Figure 9b shows the simulated 2.5-hPa temperature perturbations convolved with the

weighting function of the 667.77 cm^{-1} AIRS channel, which peaks near 2.5 hPa. As AIRS vertical coverage extends higher than the current model level, climatological temperature values from CIRA [Fleming *et al*, 1990] are used to extend the model result to the upper limit of the AIRS weighting function before convolution. While the convolved perturbation temperature is greatly diminished from the actual model output (compare Figs. 9a and 9b), the overall structure shows strong resemblance to the AIRS observation around the same time period. As the visibility limit of AIRS weighting function is ~ 12 km in vertical wavelength, gravity waves with shorter vertical wavelength (and of slower vertical group velocity) are not well detected by AIRS [Alexander and Barnet, 2006]. In the ARPS simulation, vertical wavelength of gravity waves can be as small as 7 km (Fig. 6).

4. Summary

The ARPS model is used to simulate gravity waves throughout the troposphere and stratosphere. For the 24 January 2005 case, the model generates pronounced gravity wave features over the North Atlantic region in association with geostrophic adjustment (due to enhanced anti-cyclonic curvature of the jet stream over Greenland) and possible katabatic wind down the slope of the Greenland mountainous terrain. Growing in strength and spatial coverage with altitude, wave disturbances over the Greenland are dominated by horizontal wavelengths of 80-300 km and vertical wavelength of 5-15 km. Tremendous speed reduction in the circumpolar jet occurs downstream of Greenland during the 18 hour simulation and is coincident with regions of strong wave forcing due to vertical divergence of the horizontal momentum fluxes as result of wave dissipation. Thus, the present simulation shows that gravity waves interact strongly with the polar vortex by

locally slowing down the circumpolar wind. These gravity wave features compare favorably with the AIRS radiance perturbations.

To date, details of how gravity waves interact with the stratospheric jet and their roles in ice cloud formation are still unclear. Without proper understanding of gravity waves, our ability to understand present climate and its evolution using chemistry-climate models is tenuous. *Pawson* [1997] suggested that gravity waves can trigger strong wintertime polar vortex disturbances, associated with rapid warming of the polar stratosphere. These warming events can couple with near-surface climate through their influence on the leading mode of climate variability, referred to as the “Annular Modes” [*Baldwin and Dunkerton*, 2001; *Limpasuvan et al.*, 2004]. Numerical simulations such as the one presented here can potentially allow us to better decipher such relationships between gravity waves and the vortex.

Furthermore, large temperature perturbations induced by orographic gravity waves can promote the small-scale formation of polar stratospheric clouds (PSCs) when the vortex is fairly stable (and cold) as in the present January 2005 case [*Manney et al.*, 2006]. While frigid conditions in the Antarctic polar vortex can trigger synoptic scale PSCs, the Arctic polar vortex is frequently too warm (> 190 K) for PSC formation due to continual vortex deformation and heat transport by transient planetary waves [*Pawson et al.*, 1995]. However, adiabatic cooling associated with upward propagating orographic gravity waves can generate stratospheric temperature anomalies that lead to the formation of mesoscale PSC on the lee side of mountain ranges like those in Greenland and Scandinavia [e.g. *Carslaw et al.*, 1998ab; e.g. *Dörnbrack et al.*, 2002]. Larger-scale PSCs can be induced likewise by jet-stream instabilities in breaking planetary waves [*Teitelbaum and Sadourny*, 1998; *Teitelbaum et al.*, 2001; *Hitchman et al.*, 2003]. Since

PSCs constitute localized regions of chlorine activation (“cold processing”) [Carslaw *et al.*, 1998, 1999], better understanding of PSC formation is crucial to our assessment of ozone loss.

During the Greenland case of 25-26 January 2005 reported by *Maturilli and Dörnbrack* [2006], gravity waves induced strong temperature perturbations with minimum temperature well below 190 K. Concurrent formation of PSCs over Spitsbergen was observed by ground-based lidar and simultaneous balloon-borne water vapor measurements. As shown by the green shadings of Figs. 4-6 (areas where temperature < 190 K), the ARPS results also indicate regions of possible mesoscale PSC formation as result of temperature perturbations induced by gravity waves.

The purpose of this paper is mainly to demonstrate the potential usefulness of ARPS as a tool to improve our understanding of gravity waves. In our case study, we tried to perform a simulation with the most realistic flow condition over the troposphere and the stratosphere in an effort to link the stratospheric gravity waves to their possible tropospheric sources. Moreover, with the enhanced horizontal resolution, we are able to diagnose the effects of gravity waves that are so difficult to observe. As such, usage of a forecast model such as ARPS may be prove to be valuable in (1) improving how gravity waves are parameterized in climate models and (2) directing future efforts in providing better reanalyses data in the middle atmosphere. For example, the next generation GEOS data (GEOS-5) will have horizontal resolution comparable to 50 km. As shown, in Fig. 1, this resolution is still too coarse to resolve gravity waves. Our initial comparison of model results and satellite observations may lead to improving our understanding of wave sources and characteristics.

In continuing this work, we plan to increase the horizontal resolution and vertical extension of our simulation. The higher resolution will allow for better examination of smaller scale gravity waves not resolved by the 15-km resolution and simulation at higher altitude will allow for the examination of possible wave breaking as their amplitude grows further in the mesosphere. However, both of these improvements will come with high computational cost and will further push the limit of the current numerical model, originally designed for predicting tropospheric weather

Nevertheless, the extension of ARPS into the mesosphere has proven to be successful. In their gravity wave study, *Horinouchi et al.* [2002] was able to implement the ARPS model to altitudes as high as 120 km for an idealized setup. We note that the ARPS vertical coordinate set-up differs from the MM5 used by, for example, *Wu and Zhang* [2004] and *Maturilli and Dörnbrack* [2006] for their simulations of gravity waves in the lower stratosphere (up to ~25 km). The MM5 strictly uses the sigma-coordinate, based on a reference pressure profile and the pressure values at the model top and bottom, so the terrain-following vertical coordinate value ranges between 0 to 1 [e.g. *Grell et. al.*, 1995]. In ARPS, while the lowest grid level conforms to the terrain, the vertical grid spacing can be varied and coordinate surface can be flattened above a certain height (as implemented here and discussed above) to eliminate potentially large errors associated with the calculation of horizontal gradients (like pressure gradient force terms in the governing equations) at higher altitude [*Xue et al.*, 2003]. This feature is attractive for the current types of applications.

Acknowledgements. This work was supported by the NASA/South Carolina EPSCoR Program, ASEE/NASA Faculty Fellowship Program, and NSF ATM-0213248. Support for MJA came from NASA contract #NNH04CC54C. MH and MX were supported by

NSF ATM-0129892 and ATM-0530814. Part of this work was performed at the Jet Propulsion Laboratory, California Institute of Technology, under contract with NASA. The computation for this work was performed at NASA Ames's Columbia Altrix Cluster under the support of NASA Science Mission Directorate (SMD) project Columbia. V.L. particularly thanks (1) Dr. Takeshi Horinouchi for providing initial inspiration and assistance in setting up ARPS, (2) Dr. Joe W. Waters at NASA JPL for his encouragement during this work, and (3) Mr. Marc Michelson at the University of Washington for his computing assistance.

References

- Alexander, M. J., and C. Barnet, 2006: Using satellite observations to constrain parameterizations of gravity wave effects for global models, *J. Atmos. Sci.*, in press.
- Andrews, D. G., J. R. Holton, and C. B. Leovy, 1987: *Middle Atmospheric Dynamics*, Academic Press, 489 pp.
- Aumann, H. H., and coauthors, 2003: AIRS/AMSU/HSB on the Aqua mission: design, science objectives, data products, and processing systems, *IEEE Trans. Geosci. Remote Sensing*, **41**, 253-264.
- Baldwin, M. P. and T. J. Dunkerton, 2001: Stratospheric harbingers of anomalous weather regimes, *Science*, **294**, 581-584.
- Bloom, S., A. da Silva, D. Dee, M. Bosilovich, J. D. Chern, S. Pawson, S. Schubert, M. Sienkiewicz, I. Stajner, W. W. Tan, M.-L. Wu, 2005: Documentation and Validation of the Goddard Earth Observing System (GEOS) Data Assimilation System - Version 4, *Technical Report Series on Global Modeling and Data Assimilation 104606*, **26**.
- Businger, J. A., J. C. Wyngaard, Y. Izumi and E. F. Bradley, 1971: Flux-profile relationships in the atmospheric surface layer, *J. Atmos. Sci.*, **28**, 181-189.
- Byun, D. W., 1990: On the analytical solutions of flux-profile relationships for the atmospheric surface layer, *J. Appl. Meteorol.*, **29**, 652-657.
- Carslaw, K. S., et al., 1998: Increased stratospheric ozone depletion due to mountain-induced atmospheric waves, *Nature*, **391**, 675-678.

- Carslaw, K. S., M. Wirth, A. Tsias, B. P. Luo, A. Dörnbrack, M. Leutbecher, H. Volkert, W. Renger, J. T. Bacmeister, and T. Peter, 1999: Particle microphysics and chemistry in remotely observed mountain polar stratospheric clouds, *J. Geophys. Res.*, **103**, 5785–5796.
- Chou, M-D., 1990: Parameterization for the absorption of solar radiation by O₂ and CO₂ with application to climate studies, *J. Climate*, **3**, 209-217.
- Chou, M-D. and M. J. Suarez, 1994: An efficient thermal infrared radiation parameterization for use in general circulation models, *NASA Tech Memo* 104606, 85 pp.
- Deardorff, J. W., 1980: Stratocumulus-capped mixed layers derived from a three-dimensional model, *Bound. Layer Meteor.*, **18**, 495-527.
- Dörnbrack, A. and co-authors, 2002: Evidence for inertial gravity waves forming polar stratospheric clouds over Scandinavia, *J. Geophys. Res.*, **107**, doi:10.1029/2001JD000452).
- Eckermann, S. and P. Preusse, 1999: Global measurements of stratospheric mountain waves from space. *Science*, **286**(5444), 1534-1537.
- Fetzer, E., and coauthors, 2003: AIRS/AMSU/HSB validation, *IEEE Trans. Geosci. Remote Sensing*, **41**, 418-431.
- Fleming, E. L., S. Chandra, J. J. Barnett, and M. Corney, 1990: Zonal mean temperature, pressure, zonal wind, and geopotential height as function of latitude, *Adv. Space Res.*, **10**, Issue 12, 11-59.
- Fritts, D. C. and M. J. Alexander, 2003: Gravity wave dynamics and effects in the middle atmosphere, *Rev. Geophys.*, **41**, doi:10.1029/2001RG000106.
- Grell, G., J. Dudhia, and D. Stauffer, 1995: A Description of the Fifth-Generation Penn State/NCAR Mesoscale Model (MM5). Mesoscale and Microscale Meteorology Division, NCAR/TN-398+STR, 117 pp.
- Hitchman, M. H., M. L. Buker, G. J. Tripoli, E. V. Browell, W. B. Grant, T. J. McGee, and J. F. Burris, 2003: Nonorographic generation of Arctic polar stratospheric clouds during December 1999, *J. Geophys. Res.*, **108**, 8325, doi:10.29/2001JD001034.
- Horinouchi, T., T. Nakamura, and J. Kosaka, 2002: Convectively generated mesoscale gravity waves simulated throughout the middle atmosphere, *Geophys. Res. Lett.*, **29**, doi:10.1029/2002GL016069.

- Kain, J. S. and J. M. Fritsch, 1993: Convective parameterization for mesoscale models: The Kain-Fritsch scheme, *The Representation of Cumulus Convection in Numerical Models, Meteor. Monogram*, **24**, No. 46, *Amer. Meteor. Soc.*, 165-170.
- Lilly, D. K. and E. J. Zipser, 1972: The Front Range windstorm of 11 January 1972. *Weatherwise*, **25**, 56-53.
- Limpasuvan, V., D. W. J. Thompson, and D. L. Hartmann, 2004: The life cycle of Northern Hemisphere stratospheric sudden warming, *J. Clim.*, **17**, 2584-2596.
- Lin, Y. L., R. D. Farley, and H. D. Orville, 1983: Bulk parameterization of snow field in a cloud model, *J. Clim. Appl. Meteorol.*, **22**, 1065-1092.
- Lindzen, R. S., 1981: Turbulence and stress owing to gravity wave and tidal breakdown, *J. Geophys. Res.*, **86**, 9707-9714.
- Manney, G. L., M. L. Santee, L. Froidevaux, K. Hoppel, N. J. Livesey, and J. W. Waters, 2006: EOS MSL observations of ozone loss in the 2004-2005 Arctic Winter, *Geophys. Res. Lett.*, submitted.
- Maturilli, M. and A. Dörnbrack, 2006: Polar Stratospheric Ice Cloud above Spitsbergen, *J. Geophys. Res.*, in review.
- McLandress, C., M. J. Alexander and D. Wu, 2000: Microwave limb sounder observations of gravity waves in the stratosphere: A climatology and interpretation. *J. Geophys. Res.*, **105**(D9), 11,947-11,967.
- Nappo, C., 2002: *An Introduction to Atmospheric Gravity Waves*, Academic Press, San Diego, CA, 275 pp.
- Noilhan, J., and S. Planton, 1989: A simple parameterization of land surface processes for meteorological models, *Mon. Wea. Rev.*, **117**, 536-549.
- Pawson, S., B. Naujokat, and K. Labitzke, 1995: On the polar stratospheric cloud formation potential of the northern stratosphere, *J. Geophys. Res.*, **100**, 23,215–23,225.
- Pawson, S. 1997: Effects of gravity wave drag in the Berlin troposphere-stratosphere-mesosphere GCM, in *Gravity Wave Processes: Their Parameterization in Global Climate Models, NATA ASI Ser., Ser. I*, vol. **50**, edited by K. Hamilton, pp. 327-336, Springer-Verlag (New York).
- Plougonven R., H. Teitelbaum, and V. Zeitlin, 2003: Inertia gravity wave generation by the tropospheric midlatitude jet as given by the Fronts and Atlantic Storm-Track Experiment radio soundings, *J. Geophys. Res.*, **108** (D21), 4686, doi:10.1029/2003JD003535.

Plougonven, R., and C. Snyder, 2005: Gravity waves excited by jets: Propagation versus generation, *Geophys. Res. Lett.*, **32**, L18802, doi:10.1029/2005GL023730.

Rienecker, M., 2004: File specification for GEOS-DAS gridded output version 5.3, <http://gmao.gsfc.nasa.gov/Operations/>.

Teitelbaum, H. and R. Sadourny, 1998: The role of planetary waves in the formation of polar stratospheric clouds, *Tellus*, **50A**, 302–312.

Teitelbaum, H., M. Moustououi, and M. Fromm, 2001: Exploring polar stratospheric cloud and ozone minihole formation: The primary importance of synoptic-scale flow perturbations, *J. Geophys. Res.*, **106**, 28,173–28,188.

Watanabe, S., K. Sato, and M. Takahashi, 2006: A GCM study of orographic gravity waves over Antarctica excited by katabatic winds, *J. Geophys. Res.*, in review.

Wu, D. L., 2004: Mesoscale gravity wave variances from AMSU-A radiances, *Geophys. Res. Lett.*, **28**, doi:10.1029/2004GL019562.

Wu, D. L. and F. Zhang, 2004: A study of mesoscale gravity waves over the North Atlantic with satellite observations and a mesoscale model, *J. Geophys. Res.*, **109**, doi:10.1029/2004JD005090.

Xue, M. and A. J. Thorpe, 1991: A mesoscale numerical model using the nonhydrostatic pressure-based sigma coordinate equations: model experiments with dry mountain flows, *Mon. Wea. Rev.*, **119**, 1168-1185.

Xue, M., K. K. Droegemeier, and V. Wong, 2000: The Advanced Regional Prediction System (ARPS) - A multiscale nonhydrostatic atmospheric simulation and prediction tool. Part I: Model dynamics and verification. *Meteor. Atmos. Physics*, **75**, 161-193.

Xue, M., D. Wang, J. Gao, K. Brewster, and K. K. Droegemeier, 2003: The Advanced Regional Prediction System (ARPS), storm-scale numerical weather prediction and data assimilation, *Meteor. Atmos. Phys.*, **82**, 130-170, doi:10.1007/s00703-001-0595-6.

V. Limpasuvan, Coastal Carolina University, P. O. Box 261954, Conway, SC 29528, USA. (E-mail: var@coastal.edu)

LIMPASUVAN ET AL.: STRATOSPHERIC GRAVITY WAVE SIMULATIONS

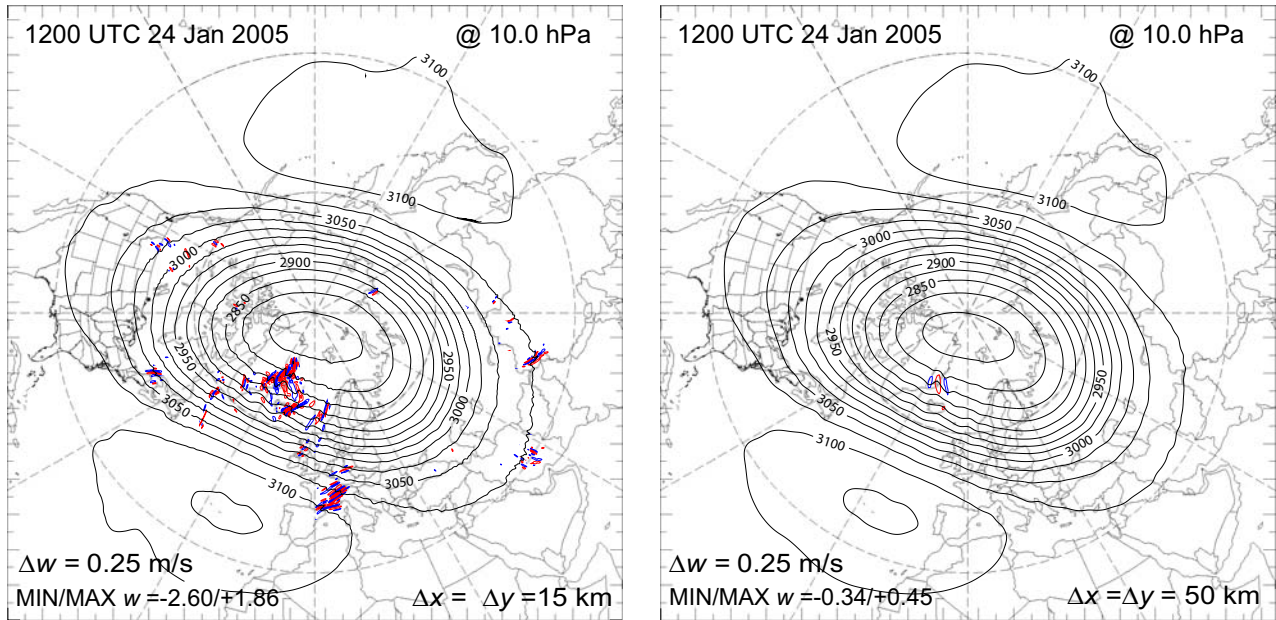


Figure 1. ARPS simulation at 1200 UTC 24 January 2005 and at 10 hPa. The geopotential height is given in black contours (every 25 dam). The vertical wind is given in color contours (every 0.25 m/s). Upward (downward) motion is shown in red (blue). Simulations from two different horizontal resolutions are shown: 15 km (left) and 50 km (right).

GEOS-4 @ 24 Jan 2005

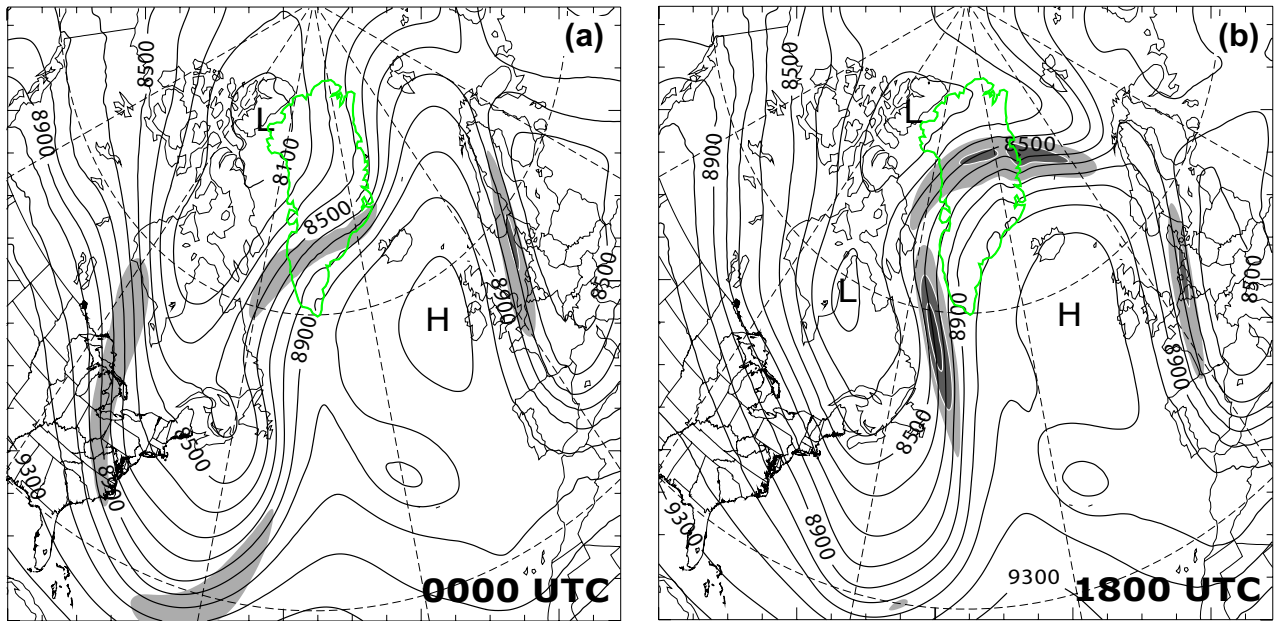
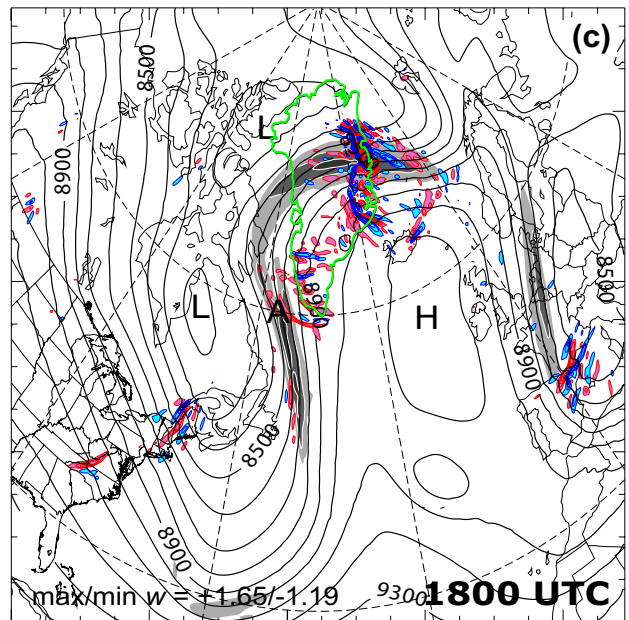
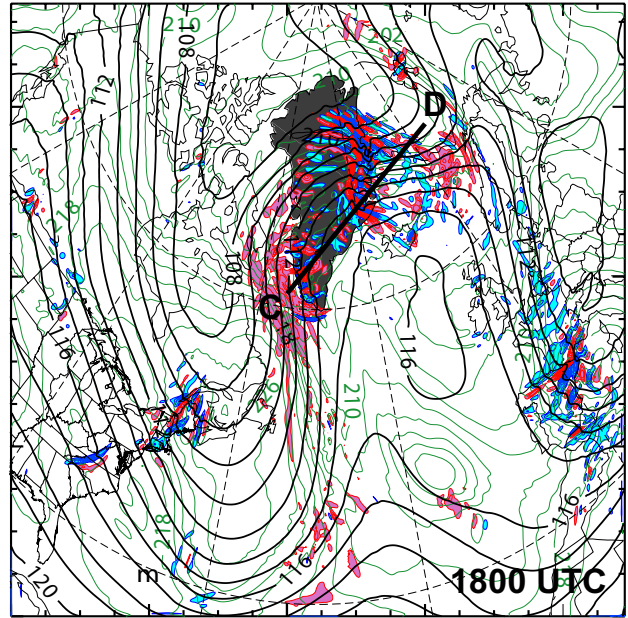
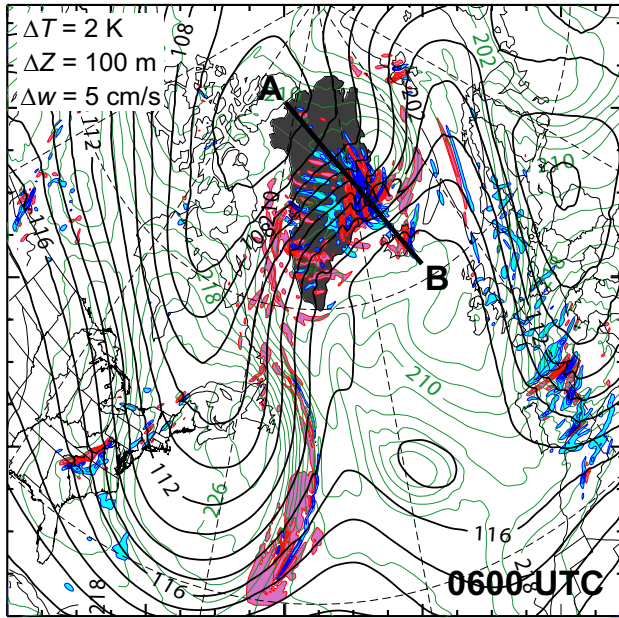


Figure 2. (a) GEOS-4 data at 0000 UTC of 24 January 2005 (initial condition). The 300-hPa geopotential height is given in black contours (every 100 m). Shaded regions show areas where the 300-hPa horizontal wind speed exceeds 60, 70, 80 m/s (darkest). (b) Same as (a) except at 1800 UTC. (c) Same as (a) except for ARPS simulation at 1800 UTC (initialized with 0000 UTC GEOS-4 data). The 80-hPa vertical wind is given in filled color contours (every 0.1 m/s). Upward (downward) motion is shown in red (blue). Greenland is outlined in green.

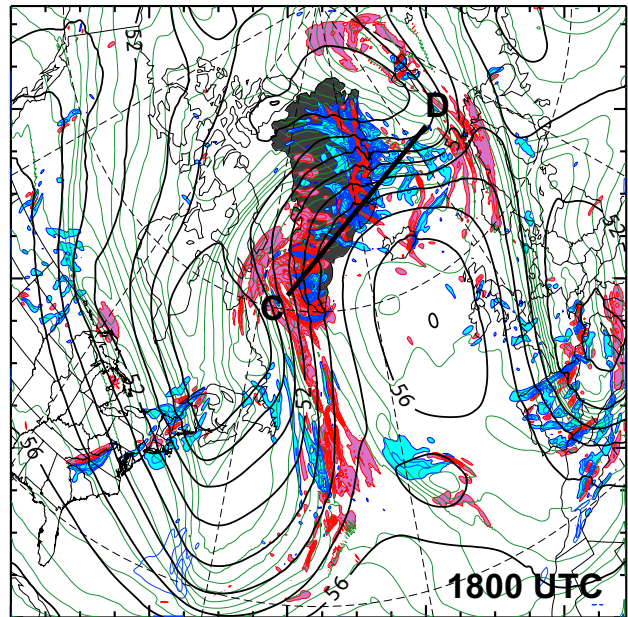
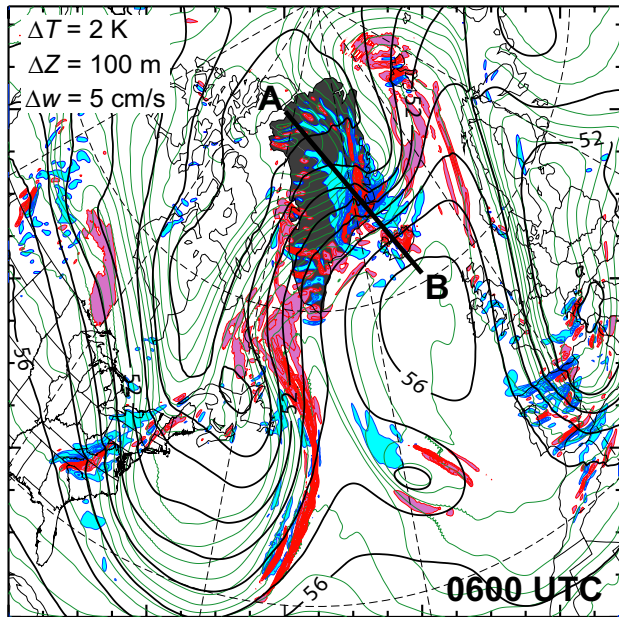
ARPS simulation @ 24 Jan 2005



200 hPa (~11.5 km)



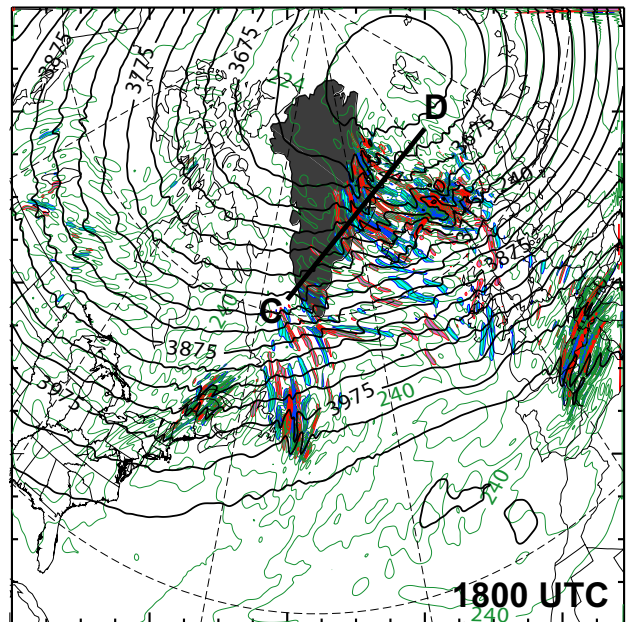
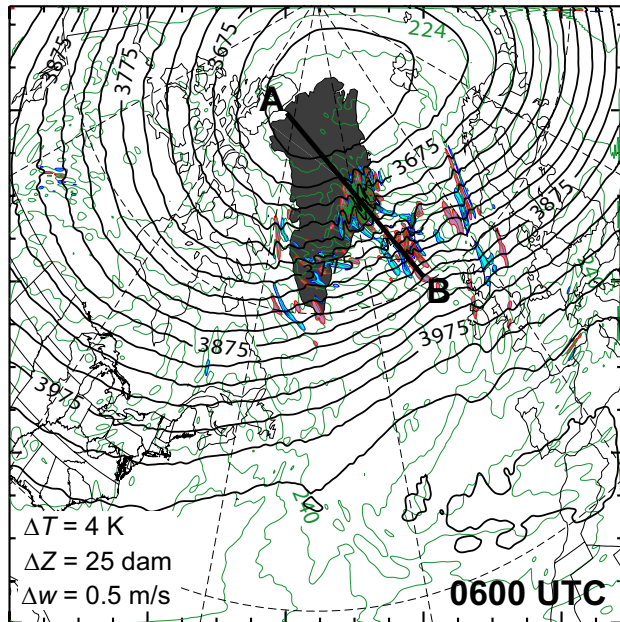
500 hPa (~5.0 km)



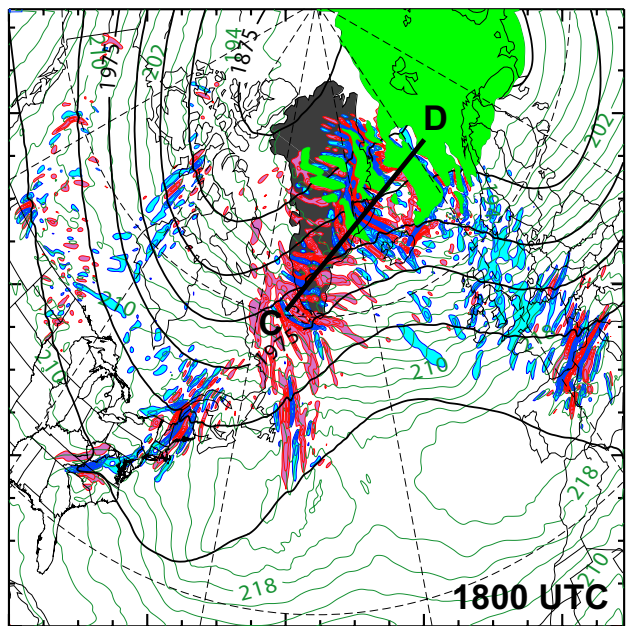
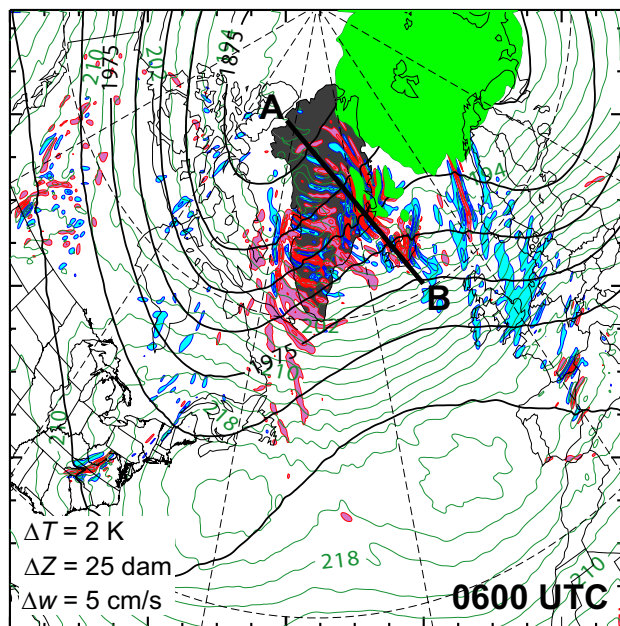
2000 km

Figure 3. (Top row) ARPS simulations at 0600 UTC and 1800 UTC of 24 January 2005 and at 200 hPa. The height field (Z) and temperature field (T) are given as black and green contours, respectively. The vertical wind (w) is given as filled color contours; upward (downward) motion is shown in red (blue). Contour intervals are indicated. (Bottom row) As above except at 500 hPa. Greenland is shaded in gray.

2.5 hPa (~42 km)



50 hPa (~22 km)



2000 km

Figure 4. Same as Figure 3 except at 2.5 and 50 hPa and regions where the temperature is lesser than 190K are shaded in green.

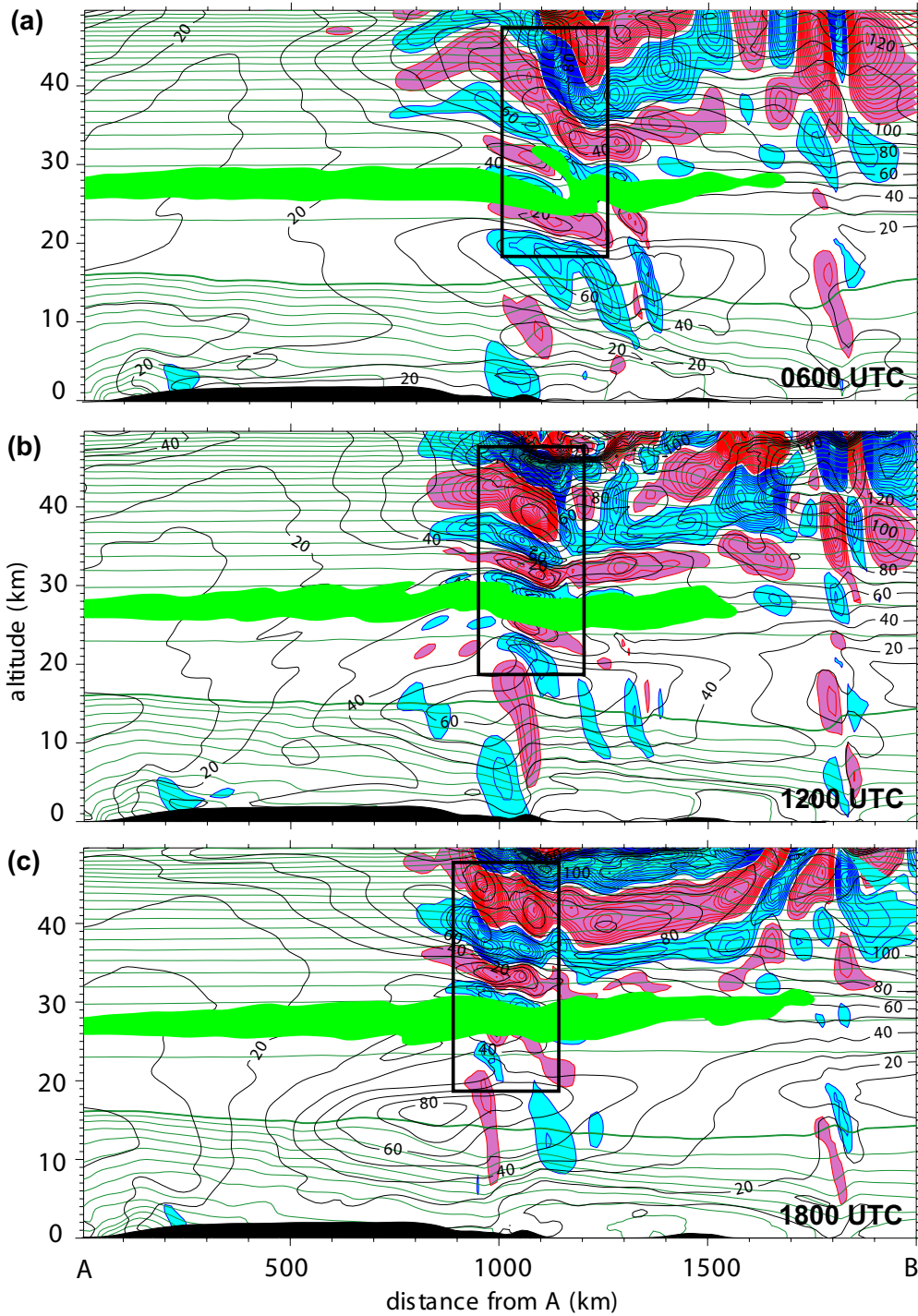


Figure 5. AB slice vertical cross-section at every six hour of the ARPS simulation. This AB slice is shown as a thick line in Figures 3 and 4. The potential temperature is shown as green contours with the thick green contour representing the 310-K value. The contour interval above (below) the thick green contour is 100 K (5 K). The total horizontal wind speed is given as black contours. The vertical wind is shown as filled color contours (every 20 cm/s). The solid black shapes at the bottom of each figure represent topography. Regions where the temperature is lesser than 190K are shaded in green.

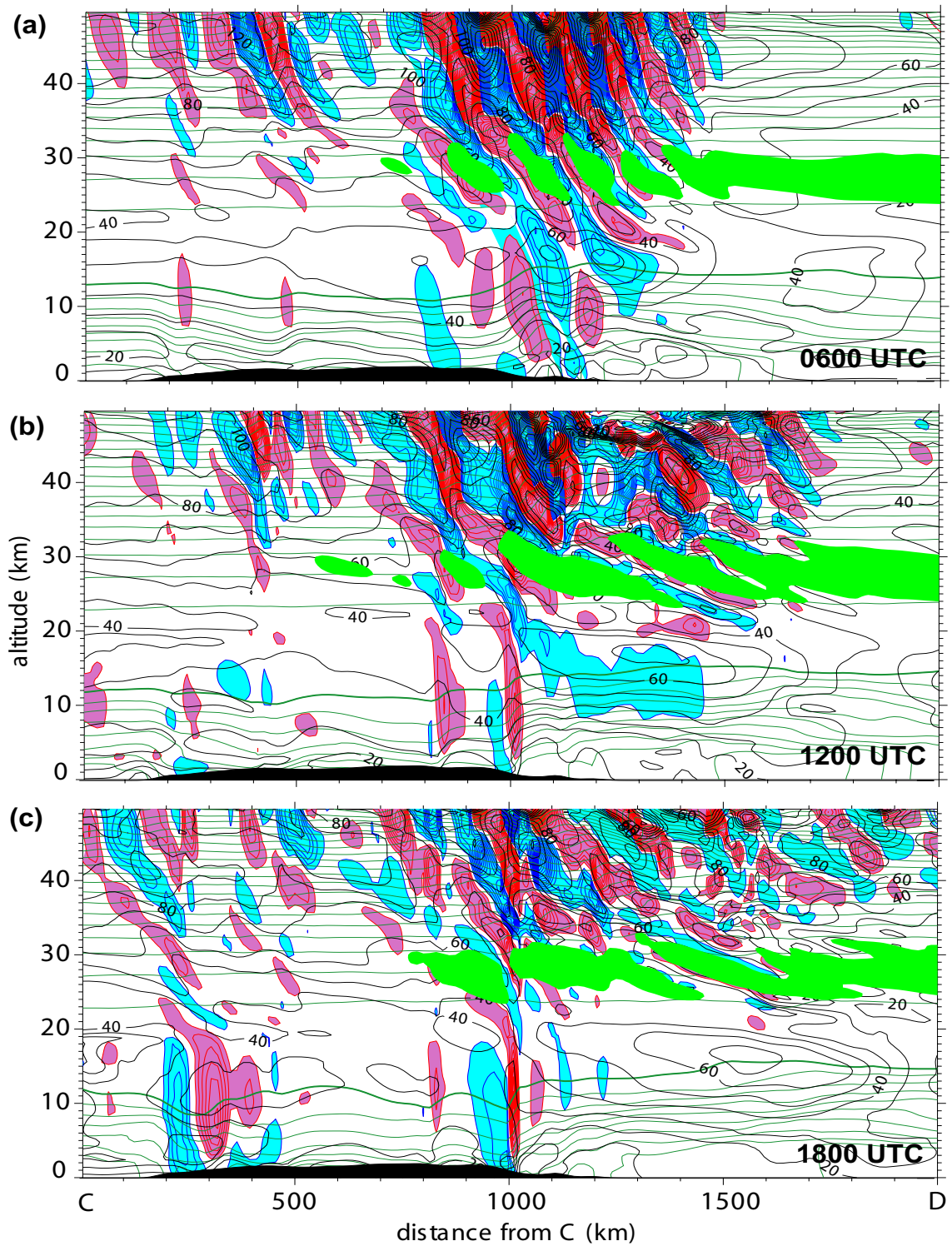
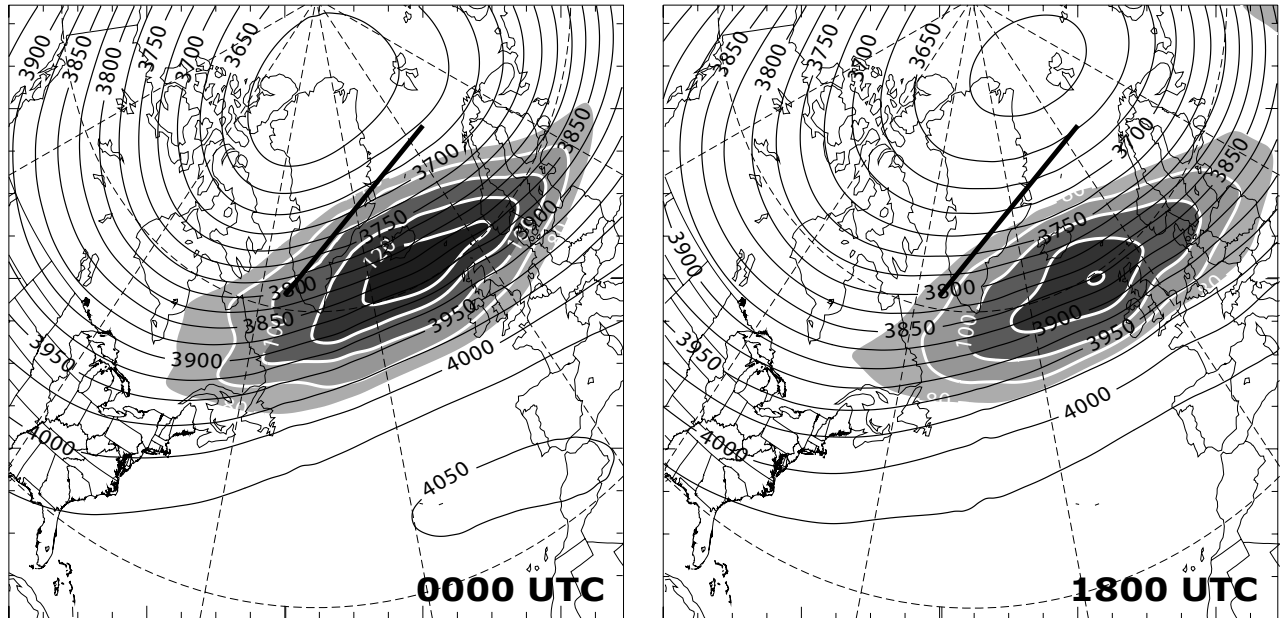


Figure 6. Same as Figure 5 except for the CD slice (shown in Figure 3 and 4).

GEOS-4 @ 24 Jan 2005



ARPS simulation @ 24 Jan 2005

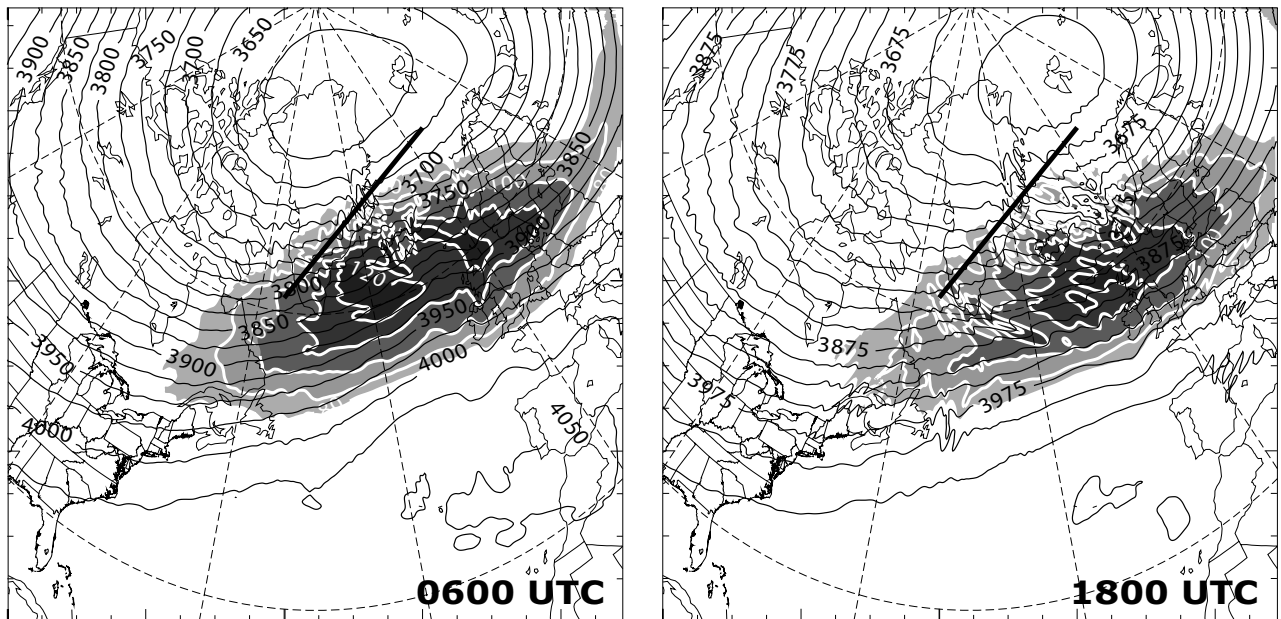


Figure 7. (Top row) GEOS-4 data at 0000 UTC (initial condition) and 1800 UTC of 24 January 2005. (Bottom row) ARPS simulation at 0600 UTC and 1800 UTC (initialized with 00 Z GEOS-4 data). The 2.5-hPa geopotential height is given in black contours (every 25 dam). Shaded regions show areas where the 2.5-hPa horizontal wind speed exceeds 80, 90, 100, 110, and 120 m/s (darkest). The thick line over Southern Greenland indicates the CD slice and is shown for reference.

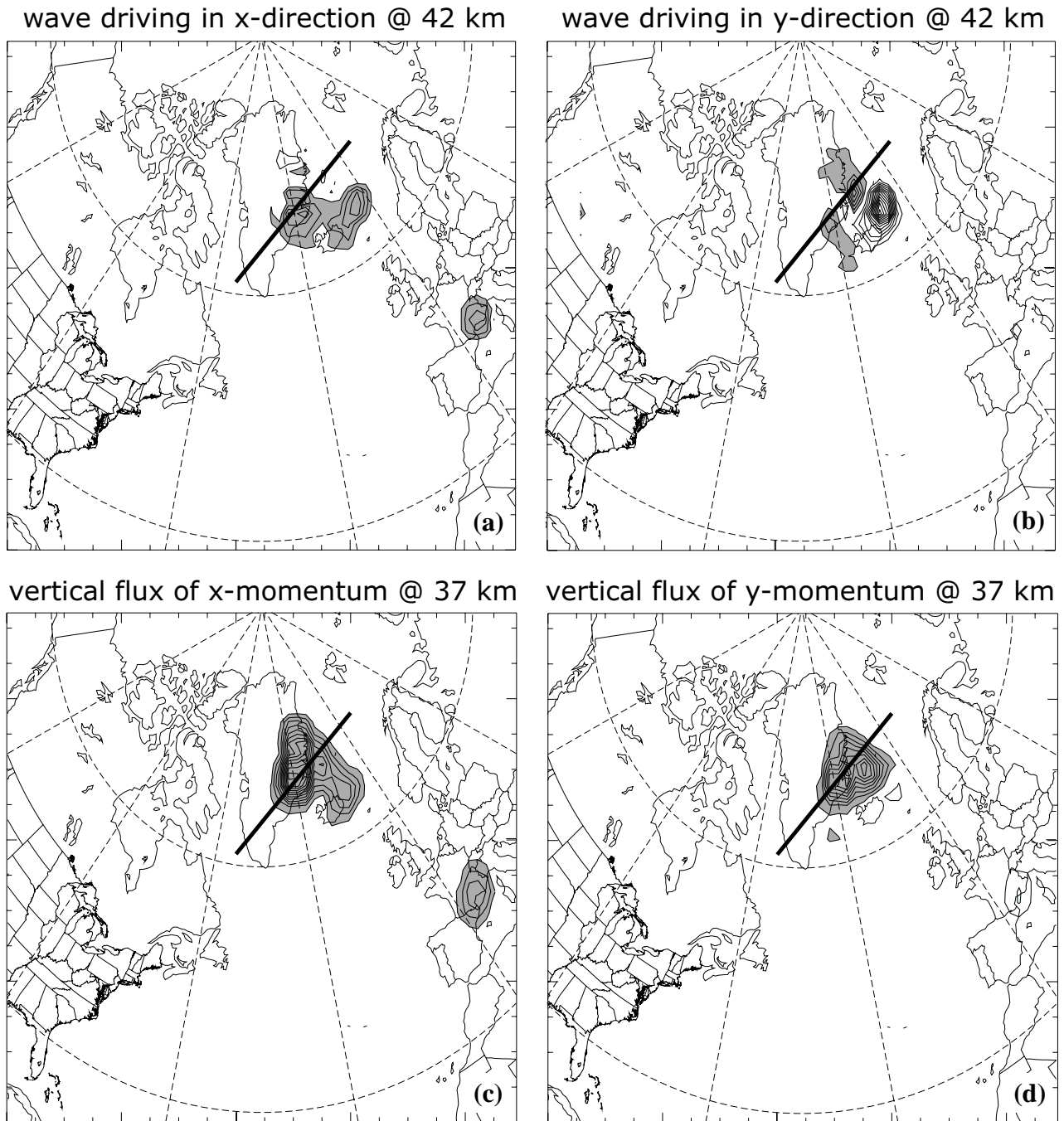
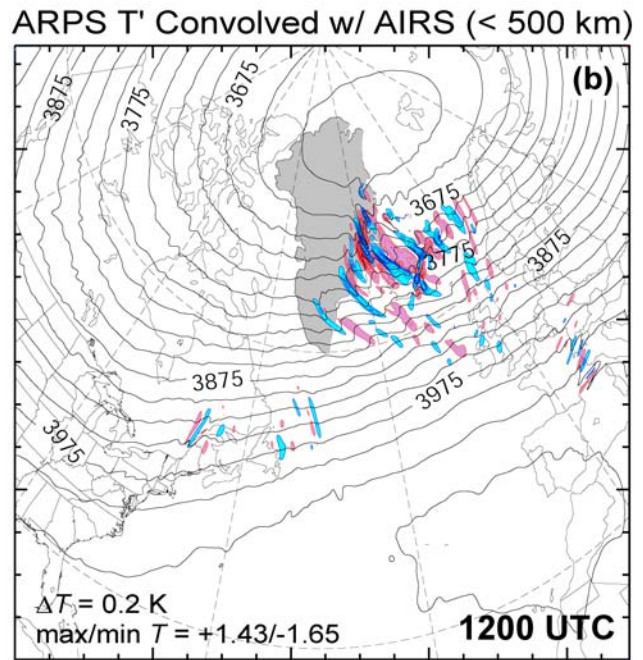
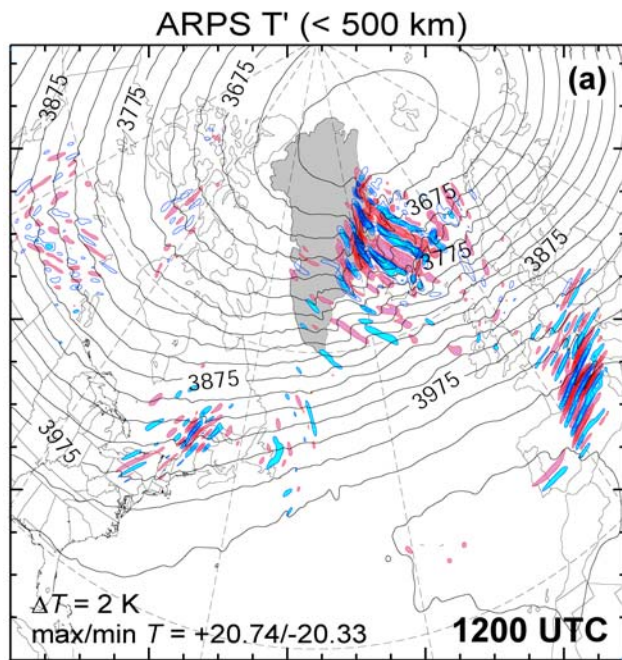


Figure 8. (a) Local wave driving in the x direction (F_x , contoured every $0.1 \text{ m s}^{-1} \text{ hour}^{-1}$) at 42 km. (b) Same as (a) except in the y direction (F_y). (c) Vertical flux of momentum in the x direction contoured every $5 \times 10^{-3} \text{ kg m}^{-1} \text{ s}^{-2}$ at 37 km (d) Same as (c) except in the y direction. All negative contours are shaded. The thick line over Southern Greenland indicates the AB slice and is shown for reference. All quantities shown are from the simulation at 1200 UTC.



AIRS Radiance Perturbation (< 500 km)
2.5 hPa, Color +/- 0.1K

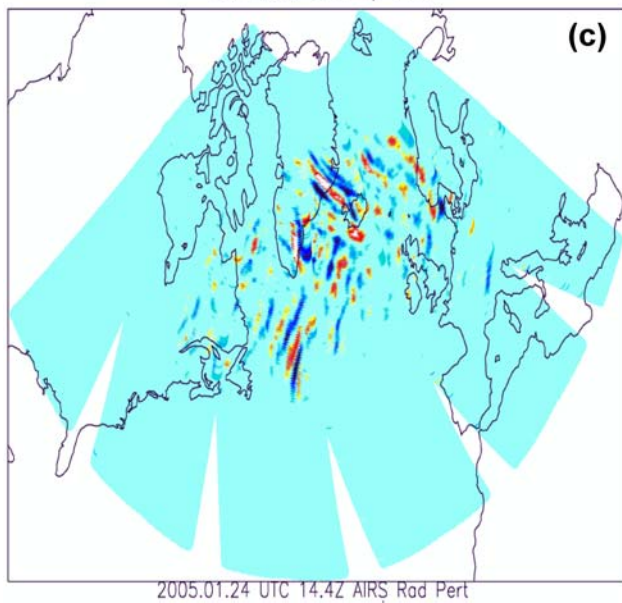


Figure 9. (a) 1200 UTC ARPS temperature (T) perturbations simulation at 2.5 hPa (contour interval indicated). Positive (negative) perturbation is shown in red (blue). The perturbation is defined as the difference between the temperature simulation at 1200 UTC and the simulation's basic state (time independent base-state of the model). The geopotential height is given in black contours (every 25 dam). Temperature perturbations of horizontal scale greater than 500 km have been removed. (b) Same as (a) except the perturbations had been convolved with the weighting function of the 667.77 cm^{-1} AIRS channel. (c) AIRS observations (ascending orbits) at 2.5 hPa of radiance perturbations (of horizontal scales shorter than 500 km).